Environmental Science & Technology

Environmental Processes

Photochemical production of sulfate and methanesulfonic acid from dissolved organic sulfur

Rachele Ossola, Julie Tolu, Baptiste Clerc, Paul Ragnar Erickson, Lenny H.E. Winkel, and Kristopher McNeill

Environ. Sci. Technol., **Just Accepted Manuscript** • DOI: 10.1021/acs.est.9b04721 • Publication Date (Web): 10 Oct 2019

Just Accepted

This document is the accepted manuscript version of the following article:
Ossola, R., Tolu, J., Clerc, B., Erickson, P. R., Winkel, L. H. E., & McNeill, K. (2019). Photochemical production of sulfate and methanesulfonic acid from dissolved organic sulfur. Environmental Science and Technology.
https://doi.org/10.1021/acs.est.9b04721

is published by the American Chemical Society. 1155 Sixteenth Street N.W., Washington, DC 20036

Photochemical production of sulfate and methanesulfonic acid from dissolved organic sulfur

Rachele Ossola[1], Julie Tolu[1,2], Baptiste Clerc[1], Paul R. Erickson[1], Lenny H. E. Winkel[1,2], Kristopher McNeill[1,]*

Author address

[1] Institute of Biogeochemistry and Pollutant Dynamics (IBP), Department of Environmental System Science, ETH Zürich, 8092 Zürich Switzerland

[2] Eawag Swiss Federal Institute of Aquatic Science and Technology, 8600 Dübendorf Switzerland

Keywords Dissolved organic sulfur, environmental photochemistry, biogeochemical cycles, sulfate, methanesulfonic acid, methanesulfinic acid, mineralization.

Abstract

Photodegradation processes play an important role in releasing elements tied up in biologically refractory forms in the environment, and are increasingly recognized as important contributors to biogeochemical cycles. While complete photooxidation of dissolved organic carbon (to CO_2), and dissolved organic phosphorous (to PO_4^{3-}) has been documented, the analogous photoproduction of sulfate from dissolved organic sulfur (DOS) has not yet been reported. Recent high-resolution mass spectrometry studies showed a selective loss of organic sulfur during photodegradation of dissolved organic matter, which was hypothesized to result in the production of sulfate. Here, we provide evidence of ubiquitous production of sulfate, methanesulfonic acid (MSA) and methanesulfinic acid (MSIA) during photodegradation of

DOM samples from a wide range of natural terrestrial environments. We show that photochemical production of sulfate is generally more efficient than the production of MSA and MSIA, as well as volatile S-containing compounds (*i.e.*, CS_2 and COS). We also identify possible molecular precursors for sulfate and MSA, and we demonstrate that a wide range of relevant classes of DOS compounds (in terms of S oxidation state and molecular structure) can liberate sulfate upon photosensitized degradation. This work suggests that photochemistry may play a more significant role in the aquatic and atmospheric fate of DOS than currently believed.

TOC art

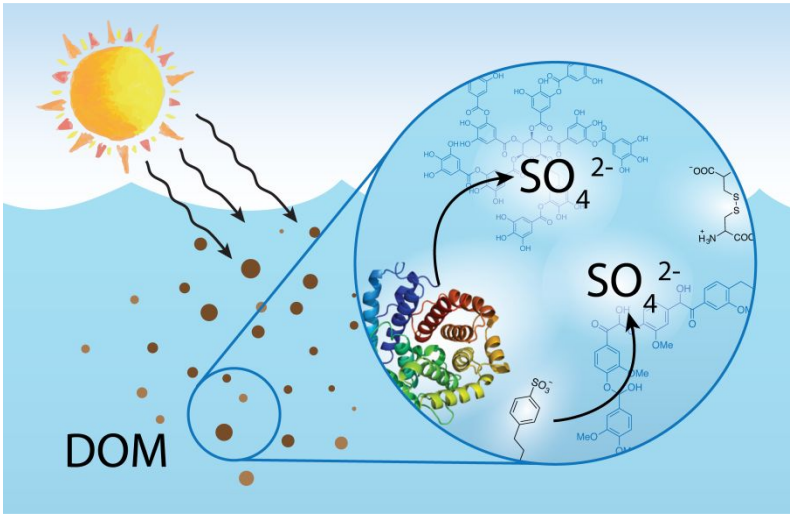

Introduction

Photochemical processes convert biologically recalcitrant organic molecules into low molecular weight compounds and inorganic species, enhancing their bioavailability and thus their mobility across environmental compartments.[1] The attention on the role of photochemistry in the biogeochemical cycles has been increasing over the last years, especially for those environments in which biological processes are inherently slow due to low temperatures, lack of water, or both.[2] For example, photodegradation of dissolved organic carbon (DOC) was reported to be responsible for 75 – 90% of the total carbon turnover in arctic lakes and rivers,[3] while in dryland systems, incorporation of photochemical processes led to substantial improvements of C-cycling models[4]. In addition, photochemistry is considered an important degradation pathway for terrestrial DOC in coastal areas, with 3 – 40% of riverine DOC input expected to be photochemically mineralized within a few years.[1,2] So far, the organic matter photomineralization studies have focused primarily on carbon, and secondarily on nitrogen and phosphorus (see reference (1)). However, we can anticipate similar processes for other elements that are part of the organic matter pool, such as sulfur.

In this context, the identification and distribution of photodegradation products is the first step to understand and quantify the role of sunlight in the biogeochemical cycles. Photochemical degradation of DOC into CO_2, CO, and a suite of low molecular weight carbonyls and carboxylates has been extensively documented in freshwater and marine environments.[1,5] Similarly, dissolved organic nitrogen (DON) is photochemically degraded to NH_4^+, primary amines, amino acids and urea,[1,6,7] while dissolved organic phosphorous (DOP) was shown to release PO_3^{4-} upon photolysis[1,8]. On the other hand, less is known about the photochemical fate of dissolved organic sulfur (DOS). So far, only carbonyl sulfide (COS) and carbon disulfide

(CS_2), have been reported as DOS photoproducts, with the majority of the studies focusing on the marine environment.[1,9] Other authors showed the formation of dimethylsulfoxide (DMSO) from the photodegradation dimethylsulfide (DMS), a volatile organosulfur compound produced by marine phytoplankton.[1,10] To the authors' knowledge, no direct evidence of the photochemical formation of sulfate from DOS has been reported so far, even if it might be anticipated based on the photochemical behavior of DOC, DON and DOP.

There is solid support for the photochemical reactivity of DOS. Studies using high-resolution mass spectrometry (HRMS) showed a high photochemical lability of sulfur-containing organic molecules from saltmarsh,[11] deep sea,[12] coastal arctic[13] and acid mine drainage[14]. These studies consistently reported faster degradation kinetics of CHOS formulas compared to CHO formulas, and observed the conversion of CHOS into CHO, implying photochemical loss of organic sulfur. Based on mass balance considerations, we hypothesized that the loss of sulfur should be associated with the formation of sulfate (photomineralization) and/or other small oxidized S-containing molecules that might elude HRMS detection. This hypothesis is further supported by the available literature on the photochemistry of DMS, COS and CS_2,[1,15] and has already been put forward by some authors[12,14]. In this work, we provide direct demonstration that non-volatile DOS undergoes facile photochemical conversion to sulfate and other small non-volatile organic compounds, such as methanesulfonic acid (CH_3SO_3H, MSA) and methanesulfinic acid (CH_3SO_2H, MSIA), under environmentally relevant conditions. Together with the enzymatic hydrolysis of sulfate esters observed in anoxic lake sediments,[16] the photochemical degradation of DOS to sulfate represents one of the few known mineralization (i.e., conversion to SO_4^{2-}) routes of organic S compounds in aquatic systems.

Materials and methods

Chemicals and organic matter samples

The twenty-two DOS model compounds, the actinometry compounds and the standards for the analyses were purchased from commercial vendors (Supplementary Text S1). The eight reference DOM samples were obtained from the International Humic Standard Society (IHSS, St. Paul, Minnesota), while the ten whole water samples were collected in several sites ranging from Switzerland (Étang de la Gruyère), to North America (Great Dismal Swamp, Lake Bradford, Prairie Pothole peat bogs) and Sweden (Storhultsmossen peat bog). More details on collection and handling of the water samples and isolates can be found in the Supplementary Texts S1 and S2.

Photodegradation experiments

The photolysis experiments were performed on reference DOM samples and on field-collected natural waters or their solid phase extracts at a concentration of ≈ 20 mg_C L^{-1} (*natural water experiments*), or on solutions containing Dismal Swamp as natural sensitizer (DS2014, ≈ 20 mg_C L^{-1}) and the selected DOS model compound (50 μmol L^{-1}) (*model compounds experiments*). The natural water experiments were performed at least in triplicates, while the model compounds experiments at least in duplicate. A summary of the initial dissolved organic carbon (DOC) and sulfate concentrations, pH and $SUVA_{254}$ values for the nineteen experimental natural water solutions is provided in Table S1. Selected DOS model compounds include thiols (cysteine, glutathione, 3-mercaptopropionic acid, 3-(methylthio)benzoic acid), thioethers (methionine, biotin, thioanisole, 3-mercaptobenzoic acid), thiophenes (2,2'-bithiophene), thioamides (thioacetamide), sulfonic acids (cysteinesulfonic acid, methanesulfonic acid, 1-hexanesulfonic

acid, 2-(cyclohexylamino)ethanesulfonic acid, taurocholic acid, benzenesulfonic acid, 4-toluenesulfonic acid, 1,2-naphthoquinone-4-sulfonic acid, 4-dodecylbenzenesulfonic acid) and organosulfate esters (pregnenolone sulfate, 4-nitrocatechol sulfate). The chemical structures are reported in the Supplementary Materials.

The experimental solutions (10 mL) were placed in cork-stoppered borosilicate test tubes (Pyrex, 15 × 85 mm, disposable) and were irradiated for 5 hours inside a photoreactor (Rayonet, Southern New England Ultraviolet Co) equipped with 6 × UVB light bulbs (Southern New England Ultraviolet Co, RPR-3000 A lamps, peak emission at 310 nm) and a turntable. During irradiation, a fan was turned on to keep the temperature constant around 30-32 °C. At each hour, an aliquot was withdrawn for quantification of sulfate via ion chromatography (IC). In the model compound experiments, MSA was also quantified via IC. For the quantification of volatile and non-volatile DOS products in the natural water experiments, an aliquot was withdrawn at the beginning and at the end of the irradiation. MSA and MSIA were quantified by HPLC-ICP-MS/MS, while volatile compounds were estimated from total S measurements via ICP-MS/MS. Total S was also measured in irradiated gas-purged solutions to assure that only non-volatile compounds were detected.

The light intensity inside the photoreactor was monitored with the chemical actinometer *p*-nitroanisole/pyridine (PNA-py).[17] A solution containing 20 μmol L^{-1} of PNA and 0.25 mmol L^{-1} of pyridine in nanopure water was irradiated for 5 hours in the experimental conditions described above. PNA and pyridine were quantified via ultra-high-performance liquid chromatography (UPLC) with UV detection. For the sulfate production experiments from DOM and model compounds, we calculated an integrated irradiance of 65 ± 4 J s^{-1} m^{-2} ($\Delta\lambda$ = 290 – 400 nm, see also Figure S1), while for experiments investigating volatile compounds, MSA and MSIA

production from natural DOM, the irradiance over the same wavelength range was 46 ± 5 J s^{-1} m^{-2}. More details can be found in the Supplementary Text S3.

Control experiments. Control experiments were also performed to unambiguously attribute sulfate, MSA or MSIA production to photochemical processes, and to show that sulfate production from DOS is in principle possible under natural sunlight (*i.e.*, at λ > ~~300~~290 nm), and in the presence of low DOC and high salts concentrations (*i.e.*, in conditions typical of marine environments). The detailed description of the control experiments is provided in the Supplementary Text S4.

Chemical analyses

Sulfate and MSA quantification via ion chromatography (IC). Sulfate and MSA were quantified via ion chromatography using either a DX-320 IC instrument (Thermo Scientific, Sunnyvale, CA, USA), or a 940 Professional IC Vario instrument (Metrohm). The DX-320 system was equipped with an EG40 eluent gradient generator, a Dionex Ion Pack AG11-HC RFIC 4 mm column and its guard column, a Dionex AERS 500 4 mm electric suppressor and an electrical conductivity detector. The sample injection volume was 250 µL, the flow rate was 1.5 mL min^{-1} and the following KOH gradient was used: 0 – 11 min, 1 mmol L^{-1}; 11 – 37 min, 1 mmol L^{-1} to 40 mmol L^{-1}; 37 to 38 min, 40 mmol L^{-1} to 1 mmol L^{-1}; 38 to 41 min, 1 mmol L^{-1}. In these conditions, sulfate was eluted at 24.0 min and had an average detection limit of 0.15 µmol L^{-1}. The Metrohm system was equipped with a Metrosep A Supp 5-250/4.0 column thermostated at 30˚C, a conductivity detector, a chemical suppressor, and was run in isocratic mode. The mobile phase was $NaHCO_3$ 0.8 mmol L^{-1} + Na_2CO_3 2.9 mmol L^{-1} prepared in nanopure water and delivered at a flow rate of 0.7 mL min^{-1}, while the sample injection volume was 100 µL. In these conditions sulfate was eluted at 25.5 min and had an average detection limit of 0.16 µmol L^{-1}.

The two IC systems provided reproducible and comparable results and were used interchangeably for sulfate detection. The DX-320 instrument was also employed for the detection of MSA in the model compounds experiments (12.5 min retention time in the conditions described above), but it was unsuitable for MSA quantification in the natural water experiments due to the relatively high detection limit (0.37 μmol L^{-1}). In addition, MSA analysis was not possible with the Metrohm IC systems as MSA co-eluted with acetate, a common DOM photolysis product.[5]

Total sulfur determination via ICP-MS/MS. Total sulfur concentrations were measured using an Agilent 8900 inductively coupled plasma – tandem mass spectrometry (ICP-MS/MS) instrument equipped with a collision/reaction cell (C/RC) (Agilent Technologies, Switzerland). We used the integrated sample introduction system (ISIS), a Micromist nebulizer, a Scott double pass spray chamber, and platinum sampler and skimmer cones. Sulfur was detected in MS/MS mode using oxygen in the C/RC. The acquisition parameters were as follows: *m/z* 32 (MS^1) - 48 (MS^2), as S formed $^{32}S^{16}O^+$ in the C/RC in presence of oxygen, integration time 0.05 ms, 1 point per peak, three replicates and 100 sweeps/replicate. All ICP-MS/MS parameters were optimized daily using a solution containing 1 μg L^{-1} of Li, Co, Y, Tl, and Ce. Only the gas flow rate and the energy discrimination were set to 30% O_2 with 2 mL min^{-1} H_2 and -8 V. An internal standard containing Sc (1 mg L^{-1}), In (1 mg L^{-1}) and Lu (1 mg L^{-1}) was used to check the stability of the signal during the runs. Quantification was done by external calibrations using standards prepared in nanopure water. The detection limit was 6 nmol L^{-1}. The natural water samples were diluted to be in the concentration range of 1.2 to 0.012 μmol L^{-1}.

MSA, MSIA, DMSO quantification via HPLC-ICP-MS/MS. Sulfur speciation analysis via HPLC-ICP-MS/MS was performed using an Agilent 1200 series HPLC pump and the Agilent 8900

ICP-MS/MS instrument described above. The chromatographic separation was performed with an Hypercarb 4.6x100 mm, particle size 5 µm column (Thermo Fisher) and an elution gradient based on changes in formic acid concentration (24 - 240 mmol L^{-1}). The mobile phase was delivered at 1 mL min^{-1} and the sample injection volume was 100 µL. As for total S quantification, S speciation was analyzed in MS/MS mode using oxygen in the C/RC, following the same tuning procedure and C/RC settings. The acquisition parameters were *m/z* 32 – 48 and an integration time of 0.05 ms. An internal standard containing Sc (5 mg L^{-1}) and Y (5 mg L^{-1}) was delivered post-column using a T-connector and the peristaltic pump of the ICP-MS/MS. ~~This allowed~~ to monitor the signal stability during the analyses. Quantification of MSA and MSIA was done by external calibrations using standards prepared in nanopure water. Detection limits were 7 nmol L^{-1} for MSA and 38 nmol L^{-1} for MSIA. The experimental samples were analyzed undiluted.

Other analyses. Total non-purgeable organic carbon (TOC) was determined using a TOC analyzer (Shimadzu Corporation). PNA and pyridine concentrations were measured with a Waters ACQUITY UPLC system equipped with a C18 column (ACQUITY UPLC BEH 130 C18, 1.7 µm; 2.1 × 150 mm) and its guard column (ACQUITY UPLC BEH C18 VanGuard Pre-column, 130Å, 1.7 µm, 2.1 mm × 5 mm). The analyses were performed in isocratic mode using a mixture of 40% acetate buffer pH 6 (+ 10% acetonitrile) and 60% acetonitrile as eluent, a flow rate of 0.15 mL min^{-1}, 5 µL injection volume and UV-Vis detection at 310 and 250 nm for PNA and pyridine, respectively. UV-Vis spectra were recorded with a Cary 100 Bio Spectrophotometer (Varian) using a 1 cm pathlength quartz cuvette in double beam mode.

Data analysis

Natural waters experiments. For each individual experiment, the concentration of photoproduced sulfate at time t ($\Delta[SO_4^{2-}]_t$) was calculated according to equation (1), where $[SO_4^{2-}]_0$ is the initial sulfate concentration (Table S1).

$$\Delta[SO_4^{2-}]_t = [SO_4^{2-}]_t - [SO_4^{2-}]_0 \quad (1)$$

For each field-collected water or reference DOM sample, $\Delta[SO_4^{2-}]_t$ values from independent triplicate experiments were averaged and the associated standard deviation was calculated. The averaged $\Delta[SO_4^{2-}]_t$ values over 5 hours of UVB irradiation were fitted with a monoexponential growth function (equation (6); see Results and Discussion) using a weighted non-linear fit (Matlab R2018b). The initial sulfate production rate ($R^0_{sulfate}$, in mmol L^{-1} h^{-1}) was calculated from the product of the fitting parameters (equation (7); see Results and Discussion). The initial sulfate production quantum yield ($\Phi^0_{sulfate}$) was obtained from the same dataset using as x-axis the absorbed photons instead of the time (Supplementary Text S5).

For the 5-hour time point, the fraction of the initial DOS converted to sulfate ($f_{sulfate,5h}$) was calculated according to equation (2).

$$f_{sulfate,5h} = \frac{\Delta[SO_4^{2-}]_{5h}}{[DOS]_0} \quad (2)$$

where $\Delta[SO_4^{2-}]_{5h}$ is the photoproduced sulfate according to equation (1) and $[DOS]_0$ is the initial DOS concentration. $[DOS]_0$ was calculated according to equation (3),[18,19] where $[S]_0$ was obtained via ICP-MS/MS and $[SO_4^{2-}]_0$ via ion chromatography, and ranged from 3.3 to 34 μmol L^{-1} (Table S2).

$$[DOS]_0 = [S]_0 - [SO_4^{2-}]_0 \quad (3)$$

The product distribution was calculated according to equation (4), where $[\text{volatiles}]_{5h} = 1 - [S]_{5h}/[S]_0$. Note that $[\text{volatiles}]_{5h}$ was set to zero if $[S]_{5h}/[S]_0$ + error ≥ 1 (the error is the standard deviation of triplicate experiments).

$$\%X = \frac{[X]_{5h}}{\Delta[SO_4^{2-}]_{5h} + [MSA]_{5h} + [MSIA]_{5h} + [\text{volatiles}]_{5h}} \quad (4)$$

Model compounds experiments. In the model compounds experiments, sulfate photoproduction was corrected for the background of the natural sensitizer (DS2014) according to equation (5).

$$[SO_4^{2-}]_{corr,t} = \Delta[SO_4^{2-}]_t - \Delta[SO_4^{2-}]_{t,DS2014} \quad (5)$$

where $\Delta[SO_4^{2-}]_{t,DS2014}$ is the photoproduced sulfate at time *t* generated from the natural sensitizer in the absence of amendments. The MSA data were not corrected due to the negligible background from the natural sensitizer in the concentration range of interest.

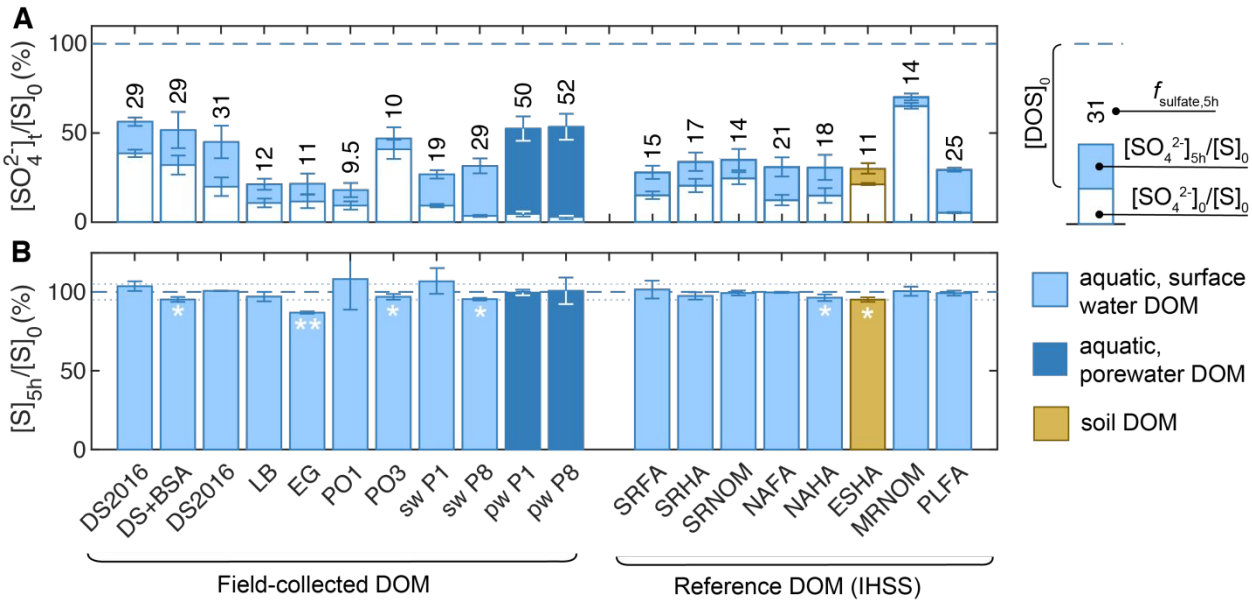

Figure 1 Photochemically induced changes in sulfur speciation in reference and field-collected DOM samples. A. White and blue bars represent $[S]_0$-normalized sulfate concentrations at the beginning and at the end of the irradiation, respectively. The numbers above the bars indicate the fraction of $[DOS]_0$ converted to sulfate after 5 hours of UVB irradiation ($f_{sulfate,5h}$). The error bars are obtained from error propagation of the standard deviations in $[S]_0$, $[SO_4^{2-}]_0$ and $[SO_4^{2-}]_{5h}$ (triplicate measurements). In these experiments, 5 hours of irradiation were approximately equivalent to 11 hours during a clear midsummer day (Supplementary Text S3; $I = 65 \pm 4$ J s^{-1} m^{-2}). **B.** Changes in total sulfur during UVB irradiation experiments. The error bars are standard deviations of independent triplicate experiments, while the asterisk(s) indicates samples with $[S]_{5h}/[S]_0$ (± error) below unity (* = value within 5%; ** = value within 10%). In these experiments, the absolute irradiance was 46 ± 5 J s^{-1} m^{-2} ($\Delta\lambda = 290 – 400$ nm). The acronyms for the waters can be found in Table S1, while the numeric values of $f_{photo,5h}$ and $[S]_{5h}/[S]_0$ and their associated experimental errors are in Table S2 and S3, respectively.

Results and discussion

Photochemical production of sulfate from DOS

Aqueous solutions of reference DOM isolates from soil, river and lakes and field-collected natural waters from lakes, swamps and peat bogs were irradiated with UVB light under laboratory conditions, and sulfate photoproduction was quantified via ion chromatography (Figure S5). This collection of materials was chosen to reflect a wide range of natural DOM variability, from terrestrially- (*i.e.*, Dismal Swamp; DS) to microbially-derived (*i.e.*, Pony Lake fulvic acid; PLFA) organic matter end members,[20,21] as can be inferred, for example, from the relatively wide range of $SUVA_{254}$ values of our samples (Table S1). We focused on freshwater environments due to the analytical challenges of detecting small sulfate variations in the large sulfate background typical of marine samples, and on the lack of easily accessible marine reference material. The lamp spectrum shows a reasonable Gaussian distribution centered around 310 nm, with a shorter wavelength cut-off of 280 nm (Figure S1). Wavelengths < 290 nm accounted only for 1.6% of total lamp irradiance, implying that the photochemical processes observed in our work are mainly triggered by environmentally relevant wavelengths.

Overall, 10 to 50% of the initial DOS was mineralized to sulfate after an irradiation period approximately equivalent to a whole clear midsummer day ($f_{sulfate,5h}$, Figure 1A), even though variations were observed across samples. Significantly higher $f_{sulfate,5h}$ values were obtained for the Prairie Pothole porewaters (50 ± 5 % and 52 ± 4 %) compared to the surface waters of the corresponding pools (19 ± 1 % and 29 ± 4 %, respectively), which exhibited photochemical behavior analogous to the other field-collected surface waters and the reference DOM samples ($f_{sulfate,5h} \approx 10 - 30\%$). Smaller variations could also be identified within the surface water samples. For instance, $f_{sulfate,5h}$ values of the Prairie Pothole surface waters, the three DS samples and PLFA were overall higher than the other samples (27 ± 4 % (N = 6) *vs* 14 ± 3 % (N = 11)). We speculate that the higher mineralized fractions in these waters may be due to specific characteristics of these three environments. Sleighter et al. showed that diagenetic sulfurization occurs in the Prairie Pothole sediments, resulting in the formation of an abundant pool of S-enriched DOM that is not found in typical lacustrine environments,[22] as confirmed by the low DOC/DOS ratios of the porewaters compared to the other samples (Table S2). Water circulation within the wetland brings the S-enriched DOS from the sediments to the surface,[22,23] where oxidative transformations can occur[11,23]. Thus, we reason that the Prairie Pothole surface waters are more reactive than common surface waters due to a higher content of organic sulfur, but less reactive than the corresponding porewaters due to a lower fraction of reduced sulfur species. Dismal Swamp is characterized by a relatively high iron content and high hydroxyl radical steady-state concentrations (during irradiation),[24] which may trigger DOS degradation mechanisms that would otherwise be of limited relevance. Finally, the higher photochemical reactivity of PLFA might be related to its molecular composition, which is dominated by bacterial- and algal-derived organic matter.[20] This difference in source material compared to

terrestrially-derived DOM might result in a different distribution of S oxidation states, an increased photochemical reactivity (already documented for triplet DOM-related processes)[25], or a combination of these two factors.

To test whether complete photomineralization can occur, long-term irradiations were also performed on PLFA and DS water (Figure 2A and S6A, respectively). Both samples showed a clear plateau in sulfate production, with a fractional yield ($Y_{sulfate}$; see below) of 67% and 85% for PLFA and DS, respectively. This result indicates that the majority, but not all, of $[DOS]_0$ could be converted to sulfate, suggesting that photorefractory (*i.e.*, photochemically stable) compounds might be present before or might be formed during irradiation. Furthermore, in PLFA, the plateau was observed when sulfate production was plotted *vs* absorbed photons (Figure 2A), while in DS the plateau was observed when using irradiation time as x-axis (Figure S6A). The difference between irradiation time and absorbed photons is related to photobleaching, i.e. the destruction of chromophores, which is a well-known process in DOM photochemistry.[26] Photobleaching was observed for both waters (Figure S6B), but appeared to limit sulfate production for PLFA only, hinting that different sulfate production mechanisms might be active in the two samples.

For more insight into the sulfate production mechanisms, we analyzed the sulfate photoproduction kinetics and tested for correlations with relevant water chemistry parameters. We fitted the sulfate concentration profiles with an exponential growth function (equation (6); Figure S5), where the pre-exponential term is proportional to $[DOS]_0$ via the constant $Y_{sulfate}$, and k is the apparent pseudo-first-order rate constant. We defined $Y_{sulfate}$ as the fractional yield of sulfate, thus the moles of sulfate produced per mole of DOS that reacts.

$$\Delta\left[SO_4^{2-}\right]_t = \left[SO_4^{2-}\right]_t - \left[SO_4^{2-}\right]_0 = [DOS]_0 Y_{sulfate}(1 - e^{-kt}) \quad (6)$$

Apparent first-order kinetic behavior is a common feature of complex chemical mixtures,[27] and has already been reported for DOC[28]. For each field-collected and reference DOM sample, the initial sulfate production rate ($R^0_{sulfate}$, in μmol L^{-1} h^{-1}), which is defined as the product of the initial rate of light absorption (R^0_{abs}) and the quantum yield of sulfate production ($\Phi_{sulfate}$), was calculated according to equation (7) using the parameters obtained from the non-linear fit.

$$R^0_{sulfate} = R^0_{abs}\Phi_{sulfate} = kY_{sulfate}[DOS]_0 \quad (7)$$

$R^0_{sulfate}$ varied among the nineteen samples both as a function of $[DOS]_0$ and as a function of the apparent rate constant (Table S2). Despite of these variations, a significant correlation was found between $R^0_{sulfate}$ and $[DOS]_0$ when excluding the porewater samples (N = 17, R^2 = 0.95; Figure 2B), revealing that the photochemical reactivity of DOS is overall comparable across a wide range of environments. The porewater samples displayed higher apparent rate constants, further confirming the high photochemical reactivity of DOS in these samples in correlation with the increased proportion of reduced S species (see above).

The same trend reported in Figure 1B was observed when the initial sulfate production quantum yield ($\Phi^0_{sulfate}$, *i.e.*, moles of sulfate produced per moles of photons absorbed) was plotted against $[DOS]_0$ (Figure S7A). The fact that $\Phi^0_{sulfate}$ (thus $R^0_{sulfate}$; see equation (7)) depends on $[DOS]_0$ can be justified considering some basic principles of photochemical kinetics. We reasoned that whether sulfate is produced via direct or indirect photolysis, its quantum yield is expected to increase linearly with $[DOS]_0$. For instance, for a generic indirect process mediated by a photochemically produced reactive intermediate (PPRI), $\Phi_{sulfate}$ can be described by the following equation.

$$\Phi_{\text{sulfate}} = \Phi_{\text{PPRI}} \cdot \frac{k_{rxn,\text{DOS}}^{\text{PPRI}}[\text{DOS}]_0}{k_d^{\text{PPRI}}} \cdot Y_{\text{sulfate}}^{\text{PPRI}} \quad (8)$$

where Φ_{PPRI} is the PPRI production quantum yield, $k^{\text{PPRI}}{}_{rxn,\text{DOS}}$ is the bimolecular rate constant for the reaction with DOS, $k^{\text{PPRI}}{}_{d}$ is the total deactivation rate constant, and $Y^{\text{PPRI}}{}_{\text{sulfate}}$ is the fractional yield of sulfate formed via reaction with PPRI. Comparable equations can be derived for direct photolysis or for a combination of direct and indirect photolysis (Supplementary Text S6).

Photochemical production of other S-containing low-molecular-weight compounds from DOS

To investigate whether other non-volatile DOS products are formed during UVB irradiation, the samples were also analyzed by high-performance liquid chromatography coupled to inductively coupled plasma – tandem mass spectrometry (HPLC-ICP-MS/MS). We found methanesulfonic acid (MSA) to be a common DOS photodegradation product, given its detection in all irradiated samples at concentrations ranging from 12.6 ± 0.8 nmol L^{-1} (PO3) to 300 ± 30 nmol L^{-1} (pw P8). Similarly, methanesulfinic acid (MSIA) was observed in seventeen out of nineteen samples at concentrations up to 10 times higher than MSA (Table S3). Furthermore, some of the samples with the highest $[DOS]_0$ showed few additional peaks in their chromatograms that were not present before irradiation (Table S3). Even though we did not identify these additional products, this result hints that sub-nanomolar concentrations of other S-containing compounds might also be produced in samples with lower $[DOS]_0$. Finally, dimethyl sulfoxide (DMSO), a known

aqueous-phase DMS photooxidation product,[1,15] was never detected after irradiation, which fits the view that DMSO is a DMS-specific photooxidation product.

Total sulfur was also quantified by ICP-MS/MS before and after UVB irradiation in order to estimate the relative importance of volatile *vs* non-volatile organosulfur products. Indeed, COS and CS_2 are the only (non-DMS) DOS photoproducts that have been reported in the literature so far.[1,19,29–33] Studies of COS and CS_2 photoproduction are mostly limited to coastal and open ocean environments, with a single work investigating a freshwater system (an artificial lake).[9] Based on this latter publication and on mechanistic studies showing COS production from the DOM-photosensitized degradation of cysteine, glutathione and other thiols,[34–38] which are ubiquitous compounds in the environment (Table S4 and references therein), we anticipated that these volatile compounds should also be formed (and lost to the headspace) during our irradiation experiments. The resulting mass balances, expressed as $[S]_{5h}/[S]_0$ ratio, were complete for most of the samples, indicating that COS and CS_2 were at most minor products (Table S3 and Figure 1B). The only notable exception was the samples collected from Étang de la Gruère, which had a $[S]_{5h}/[S]_0$ value considerably lower than unity (0.87 ± 0.01). Unfortunately, the relatively high experimental error of our method provides only an estimate of the contribution of volatile species to the inventory of DOS photoproducts. Future studies based on direct gas measurements would be needed to accurately quantify photochemical production of COS and CS_2 in freshwater environments.

In order to understand the relative importance of each degradation pathway, we estimated the product distribution in each DOM sample (Figure 2C and Table S3). Note that, due to the relatively high experimental errors, volatile product contributions were considered only if $[S]_{5h}/[S]_0$ + error < 1. Overall, sulfate was the main photoproduct, representing 28 – 94% of the

reacted DOS pool, with a median value of 75%. MSIA and MSA were 0 – 39% (median: 14%) and 1.2 – 8% (median: 3.4%) of the products, respectively. In the six (of nineteen) samples where the mass balance was significantly different from 100% (indicating that S was lost to volatile products) the volatile species represented 15 – 71% of the reacted pool (median: 34%). These results mirror the behavior of DOC, as CO_2, the highest oxidation state product, is released approximately 2 to more than 65 times more effectively than CO, the second most abundant DOC photoproduct.[39]

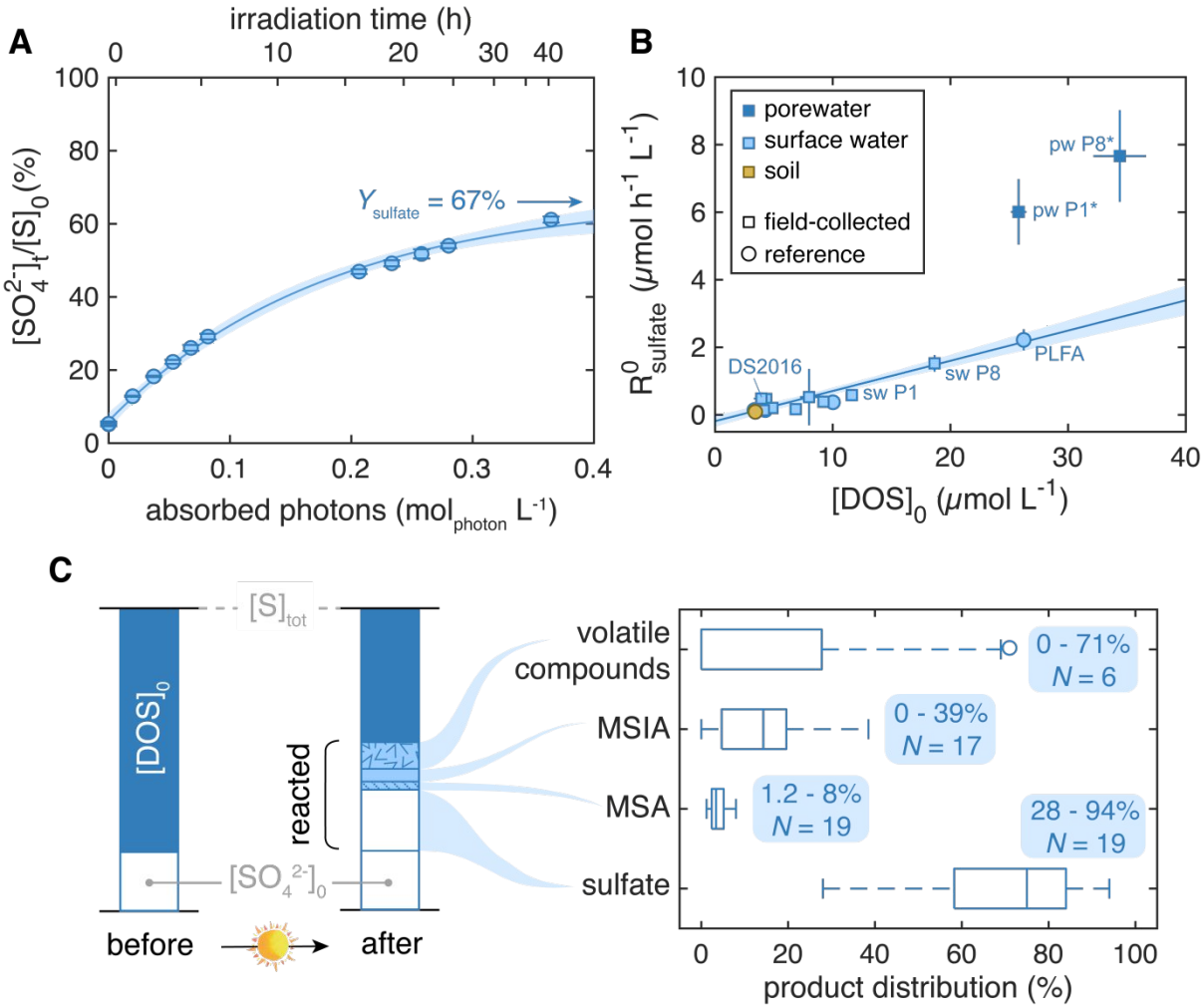

Figure 2 Long-term PLFA degradation kinetics, and sulfate, MSA and MSIA production from naturally-occurring DOS. A Long-term photomineralization for PLFA. The derivation of the lower x-axis (absorbed photons) is described in the Supplementary Text S5. The error bars are standard deviations of triplicate experiments. **B** Linear regressions of $R^0_{sulfate}$ *vs* $[DOS]_0$ for

the field-collected (squares) and reference (circles) surface water and soil DOM (R^2 = 0.95, N = 17, slope = (0.089 ± 0.005) h^{-1}). The porewater samples (blue filled squares) are excluded from the fit. When not visible, the error bars are within the symbols. Numerical values of $R^0_{sulfate}$ and $[DOS]_0$ and their associated errors are listed in Table S2. **C** Box plot showing the products distribution for the nineteen samples investigated. The numbers in blue show the ranges for each single product, while N indicates the number of DOM samples in which the product was observed after irradiation. The numerical values for each DOM sample are listed in Table S3.

Environmentally relevant molecular precursor of sulfate and MSA

To identify possible molecular precursor substrates for sulfate and MSA production, twenty-two organic sulfur model compounds (Figure S8) were irradiated with UVB light in the presence of a natural sensitizer (Dismal Swamp water), and both sulfate and MSA were quantified via ion chromatography (Table 1 and Figure S9). The model compounds were selected based on the oxidation state of the S atom(s) and the aliphatic/aromatic nature of the carbon scaffold. Specifically, we focused on the three most abundant S oxidation states found in natural organic matter (Figure S10 and references therein), namely S(-II) (thiols, thioethers and thiophenes), S(+IV) (sulfonic acids) and S(+VI) (organosulfates). For each S oxidation state, several aromatic and aliphatic compounds were selected in order to test whether the molecular structure influences the photochemical fate of the S atom(s). Altogether, this collection of model compounds includes molecules that have already been detected in the environment or that might be present in DOS with a modified carbon scaffold (Tables S4-S5).

Table 1 Photosensitized production of sulfate and MSA from individual model compounds. Summary of sulfate and MSA concentrations detected after 2 hours of UVB irradiation (I_λ = 65 ± 4 J s^{-1} m^{-2}) in the presence of an individual model compound (50 µmol L^{-1}) and a natural sensitizer (Dismal Swamp water). The molecular structures are provided in Figure S8, and the 5-hour irradiation kinetics in Figure S9. N.D. = no peak detected; N.S. = non-significant ($[SO_4^{2-}]_{corr,2h}$ < 0.0 ± 0.2 µmol L^{-1}). [a] Hybridization of carbon atoms bound to sulfur referred to as aliphatic (sp^3) or aromatic (sp^2) in the main text. [b] Corrected for the sulfate produced by the natural sensitizer. [c] + = detected in the environment (references in Table S4); * = surrogate for S-containing functional groups present in environmental systems (see Table S5 for examples). [d] 50 mg_C L^{-1} addition of bovine serum albumin is equivalent to ≈ 25 μmol_S L^{-1}.

399

Compound	C hybridization [a]	$[SO_4^{2-}]_{corr,2h}$ (µmol L^{-1}) [b]	$[MSA]_{2h}$ (µmol L^{-1})	Environmental occurrence [c]
S(-II): Thiols, thioethers and thiophenes				
Cysteine	sp^3	**2.2** ± 0.2	N.D.	+
Methionine	sp^3	**1.87** ± 0.03	**1.97** ± 0.02	+
Glutathione	sp^3	**2.5** ± 0.4	N.D.	+
Bovine serum albumin [d]	sp^3	**1.1** ± 0.4	N.D.	*
3-Mercaptopropionic acid	sp^3	**1.08** ± 0.02	N.D.	+
Biotin	sp^3	**2.6** ± 0.2	N.D.	+
Thioacetamide	sp^2	**7.3** ± 0.3	N.D.	*
3-(Methylthio)benzoic acid	sp^2/sp^3	**0.25** ± 0.05	**4.5** ± 0.8	*
Thioanisole	sp^2/sp^3	**1.00** ± 0.02	**0.62** ± 0.01	+
3-Mercaptobenzoic acid	sp^2	**3.4** ± 0.3	N.D.	*
2,2'-Bithiophene	sp^2	**20** ± 3	N.D.	*
S(+IV): Sulfonic acids				
Cysteinesulfonic acid	sp^3	N.S.	N.D.	*
Methanesulfonic acid	sp^3	N.S.	N.D.	+
1-Hexanesulfonic acid	sp^3	N.S.	N.D.	*
2-(Cyclohexylamino)ethane sulfonic acid	sp^3	N.S.	N.D.	*
Taurocholic acid	sp^3	N.S.	N.D.	*
Benzenesulfonic acid	sp^2	**1.5** ± 0.1	N.D.	*
4-Toluenesulfonic acid	sp^2	**4.3** ± 0.2	N.D.	+
1,2-Naphthoquinone-4-sulfonic acid	sp^2	**35** ± 2	N.D.	*
4-Dodecylbenzenesulfonic acid	sp^2	**1.2** ± 0.1	N.D.	+
S(+VI): Organosulfates				
Pregnenolone sulfate	-	**3.0** ± 0.1	N.D.	*
4-Nitrocatechol sulfate	-	**3.7** ± 0.1	N.D.	*

400

401 Nearly all model compounds could be photomineralized to sulfate, albeit with different kinetics
402 and different yields (Figure S9). The aliphatic sulfonic acids were the only molecules that
403 showed no sulfate production. In two cases (cysteinesulfonic acid and MSA), we could

experimentally confirm the photochemical stability of the parent compound ($[MSA]_{5h}/[MSA]_{0h}$ = 1.00 ± 0.06; $[CysSO_3H]_{5h}/[CysSO_3H]_{0h}$ = 1.03 ± 0.04), providing good support for the hypothesis that the incomplete conversion of DOS to sulfate can also be due to the initial presence and/or formation of photochemically stable DOS components. Such photorecalcitrant molecules can be produced from biological activity (i.e. cysteinesulfonic acid)[40] or could be formed during DOS photodegradation (i.e. MSA). In addition, MSA was always formed during the photodegradation of methyl thioethers, suggesting that methionine and other naturally occurring methyl thioethers can be the precursors of MSA. In one case, MSA was produced in higher yields than sulfate (3-(methylthio)benzoic acid: $[SO_4^{2-}]_{corr,2h}$ = 0.25 ± 0.05 μmol L^{-1}; $[MSA]_{2h}$ = 4.5 ± 0.8 μmol L^{-1}), reinforcing the idea that sulfate is not necessarily the only photodegradation product of DOS.

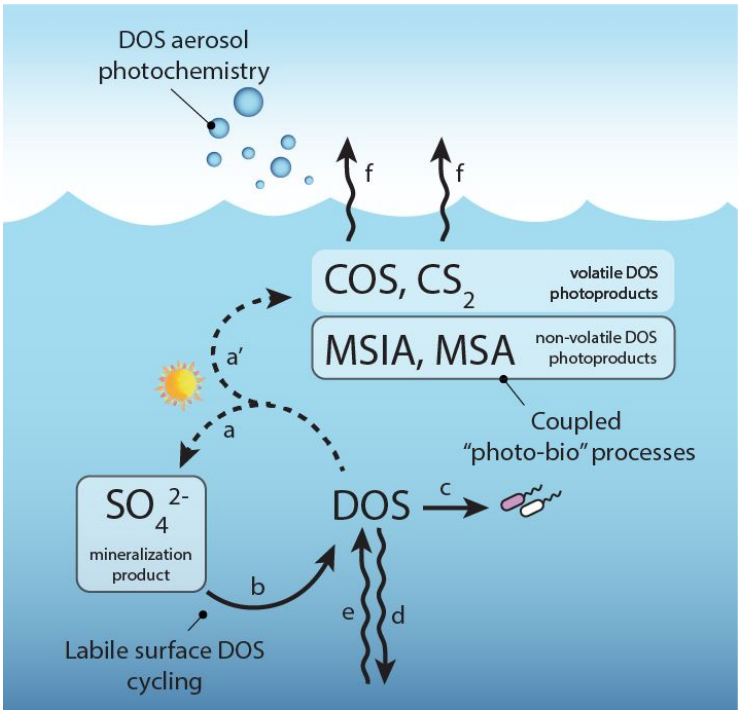

Figure 3. Overview of the photochemically induced DOS cycle in sunlit surface waters and possible implications for DOS biogeochemistry. The dotted lines represent photochemical processes. The photoproducts identified for the first time in this study are in black-framed boxes.

Legend: *a.* photomineralization; *a'.* photofragmentation; *b.* sulfate assimilation and DOS release from phytoplankton; *c.* microbial DOS uptake; *d*. downwelling; *e*. upwelling; *f.* outgassing.

Implications and open questions

Our study reports direct evidence of sulfate production from the photochemical degradation of dissolved organic sulfur from a variety of natural freshwater samples (Figure 3). This finding fills in the general picture of the role of photochemistry on the biogeochemical cycle of the main elements, showing that, similar to dissolved organic carbon,[1] nitrogen[6,7] and phosphorous[8], also DOS can be converted to its inorganic form via photochemical routes.

In addition, the identification of a photomineralization mechanism provides a more complete picture on the biogeochemistry of DOS. Only few studies on DOS photodegradation can be found in the literature,[11,12,14] which focused on the loss of DOS formulas via HRMS, and not on the identification of the S-containing products. The inverse is true for the studies of photochemical formation of COS and CS_2 in the natural environment,[1,19,29–33] which described the appearance of products with no clear link made to loss of DOS. Our work provides a bridge between these two research themes. First, it suggests that sulfate is the most likely product associated to the loss of DOS observed in the HRMS studies. For instance, Gomez-Saez et al. reported up to ≈ 30% of $[DOS]_0$ loss after 2 days of solar irradiation in saltmarsh porewater samples. Even though care should be taken when comparing results obtained with different light sources, this number qualitatively agrees with the high mineralized fractions (i.e. DOS conversion to sulfate) that we observed for our porewater samples ($f_{photo,5h}$ = 50 – 52%). Second, the present work gives a sense of the relative importance of the different degradation pathways. In particular, we found that sulfate is often the main photodegradation product, while the other volatile (COS, CS_2) and non-volatile (MSA, MSIA) low-molecular-weight compounds are

443 quantitatively less important in terms of mass balance. These results echo the observation that
444 CO_2, the most oxidized carbon form, is the most abundant DOC photodegradation product.[1] Our
445 results are directly relevant to aquatic terrestrial organic matter in freshwater systems, but we
446 expect them to hold valid also for marine DOM. Control experiments showed no suppression in
447 sulfate production at high ionic strength and low DOC concentrations, which are conditions
448 typical of marine environments (Supplementary Text S4). In addition, preliminary results with a
449 marine DOM sample collected in the Pacific Ocean were found in good agreement with the
450 findings presented in this work for terrestrial DOM and for Pony Lake fulvic acid
451 (Supplementary Text S4), which has been used by other authors as a surrogate for marine
452 DOM[21]. As a further point, model compounds able to produce both sulfate and COS are present
453 in both terrestrial and marine environments (Table S4). For instance, glutathione, which can
454 produce both COS[35,38] and sulfate (see above), is commonly found in freshwater,[41] estuaries[42]
455 and in the open ocean[43]. Nevertheless, further studies need to experimentally confirm the
456 production of sulfate and non-volatile low-molecular-weight compounds from marine DOS
457 photolysis.

458 The facile conversion of DOS to sulfate and MSA described here puts the DOS cycle into a new
459 perspective, providing possible answers to the many unresolved questions on its biogeochemistry
460 and suggesting new research directions (Figure 3). For example, photomineralization can be a
461 potential explanation for the fast DOS turnover described by Ksionzek et al. in the mixed surface
462 layer of the ocean.[18] In particular, we anticipate that autochthonous DOS released by
463 phytoplankton at the surface (i.e. glutathione and other peptides) can be converted to sulfate
464 upon DOM-sensitized photolysis. In addition, photochemistry can play a role in converting
465 biologically refractory DOS components into bioavailable substrates, similarly to what happens

for carbon cycling.[1,44] Indeed, microorganisms able to use MSA either as a S-source, a C-source or an energy source have been identified in a variety of environments[45,46] and were recently found to be abundant in surface seawater[47]. Lastly, we hypothesize that non-DMS sulfur compounds present in aerosols, such as organosulfates,[48] cysteine- and methionine-containing peptides and proteins,[49] might degrade to sulfate via aqueous-phase photochemical reactions sensitized by organic chromophores, similar to what we report here for bulk solutions. Thus, atmospheric DOS might be an aqueous-phase precursor of non-sea-salt sulfate, an important contributor to aerosol formation in remote marine areas.[50,51] Photosensitized oxidations can also represent an additional route to convert other atmospherically relevant inorganic S species, such as SO_2/SO_3^{2-}, to sulfate (Figure S11). This photosensitized process, together with other water-phase reactions involving reactive nitrogen species,[52,53] might contribute to the high sulfate levels observed during severe urban haze events, which cannot be justified by gas phase reactions only.[54] Future work is needed to assess the importance of DOS photodegradation in the ocean surface and in the atmosphere.

ASSOCIATED CONTENT

Supporting information

Material suppliers and water collection procedures; details of solid phase extraction procedures; description of the control experiments; actinometry calculations and theoretical derivation of $\Phi_{sulfate}$; lamp spectra; supplementary figures on sulfate production kinetics from natural waters and DOS model compounds; molecular structures of DOS model compounds; literature overview of DOS speciation data from XANES analysis; preliminary results on the photochemical degradation of sulfite to sulfate; numerical values of initial total sulfur, DOC,

sulfate, pH, $SUVA_{254}$ of the natural water samples; numerical values of initial rates of sulfate production, initial sulfate production quantum yields, photoproducts distributions; overview of environmental occurrence of DOS model compounds.

Abbreviations

COS, carbonyl sulfide; CS_2, carbon disulfide; DMS, dimethylsulfide; DMSO, dimethylsulfoxide; DOC, dissolved organic carbon; DOM, dissolved organic matter; DOS, dissolved organic sulfur; DS, Dismal Swamp; HRMS, high-resolution mass spectrometry; MSA, methanesulfonic acid; MSIA; methanesulfinic acid; PLFA, Pony Lake fulvic acid; PPRI, photochemically produced reactive intermediate.

AUTHOR INFORMATION

Corresponding Authors

* kris.mcneill@env.ethz.ch

Author Contributions

R.O., P.R.E., J.T., L.H.E.W. and K.M. designed the experiments. R.O. and B.C. performed the irradiation experiments, the IC and UPLC analyses. J.T. performed the ICP-MS/MS and the HPLC-ICP-MS/MS analyses. R.O. analyzed the data and wrote the manuscript with contributions from P.R.E., J.T., L.H.E.W. and K.M..

Funding sources

The authors acknowledge ETH Zurich for funding.

Acknowledgements

The authors thank Dr. N. Borduas-Dedekind for the fruitful discussions on the atmospheric chemistry implications of the study. We acknowledge Prof. Dr. M. H. Schroth and B. Studer for the instrumental support on the ion chromatography analyses, and Dr. G. Getzinger for the optimization of the solid phase extraction procedures of the Prairie Pothole samples. We thank Prof. Dr. K. Mopper for the collection of Dismal Swamp water (2014), Dr. V. S. Lin also for the collection of Dismal Swamp water (2016), Dr. C. Chu, C. A. Davis, Dr. E. Janssen and M. Schmitt for the collection of water from Étang de la Gruère, Dr. M. Sander, N. Walpen, Dr. G. Getzinger and Prof. Dr. M. H. Schroth for the collection of the Storhultsmossen pool water samples, and Prof. Dr. W. Arnold and his group for having provided the surface and porewater samples from the Prairie Pothole wetlands.

References

(1) Mopper, K.; Kieber, D. J.; Stubbins, A. Chapter 8 - Marine Photochemistry of Organic Matter: Processes and Impacts A2 - Hansell, Dennis A. In *Biogeochemistry of Marine Dissolved Organic Matter (Second Edition)*; Carlson, C. A., Ed.; Academic Press: Boston, 2015; pp 389–450.

(2) Sulzberger, B.; Austin, A. T.; Cory, R. M.; Zepp, R. G.; Paul, N. D. Solar UV Radiation in a Changing World: Roles of Cryosphere–Land–Water–Atmosphere Interfaces in Global Biogeochemical Cycles. *Photochem. Photobiol. Sci.* **2019**, *18* (3), 747–774. https://doi.org/10.1039/C8PP90063A.

(3) Cory, R. M.; Ward, C. P.; Crump, B. C.; Kling, G. W. Sunlight Controls Water Column Processing of Carbon in Arctic Fresh Waters. *Science* **2014**, *345* (6199), 925–928. https://doi.org/10.1126/science.1253119.

(4) Adair, E. C.; Parton, W. J.; King, J. Y.; Brandt, L. A.; Lin, Y. Accounting for Photodegradation Dramatically Improves Prediction of Carbon Losses in Dryland Systems. *Ecosphere* **2017**, *8* (7), e01892. https://doi.org/10.1002/ecs2.1892.

(5) Moran, M. A.; Zepp, R. G. Role of Photoreactions in the Formation of Biologically Labile Compounds from Dissolved Organic Matter. *Limnol. Oceanogr.* **1997**, *42* (6), 1307–1316. https://doi.org/10.4319/lo.1997.42.6.1307.

(6) Bushaw, K. L.; Zepp, R. G.; Tarr, M. A.; Schulz-Jander, D.; Bourbonniere, R. A.; Hodson, R. E.; Miller, W. L.; Bronk, D. A.; Moran, M. A. Photochemical Release of Biologically Available Nitrogen from Aquatic Dissolved Organic Matter. *Nature* **1996**, *381* (6581), 404–407. https://doi.org/10.1038/381404a0.

(7) Vähätalo, A. V.; Zepp, R. G. Photochemical Mineralization of Dissolved Organic Nitrogen to Ammonium in the Baltic Sea. *Environ. Sci. Technol.* **2005**, *39* (18), 6985–6992. https://doi.org/10.1021/es050142z.
(8) Gardolinski, P. C. F. C.; Worsfold, P. J.; McKelvie, I. D. Seawater Induced Release and Transformation of Organic and Inorganic Phosphorus from River Sediments. *Water Res.* **2004**, *38* (3), 688–692. https://doi.org/10.1016/j.watres.2003.10.048.
(9) Du, Q.; Mu, Y.; Zhang, C.; Liu, J.; Zhang, Y.; Liu, C. Photochemical Production of Carbonyl Sulfide, Carbon Disulfide and Dimethyl Sulfide in a Lake Water. *J. Environ. Sci.* **2017**, *51* (Supplement C), 146–156. https://doi.org/10.1016/j.jes.2016.08.006.
(10) Uher, G.; Pillans, J. J.; Hatton, A. D.; Upstill-Goddard, R. C. Photochemical Oxidation of Dimethylsulphide to Dimethylsulphoxide in Estuarine and Coastal Waters. *Chemosphere* **2017**, *186* (Supplement C), 805–816. https://doi.org/10.1016/j.chemosphere.2017.08.050.
(11) Gomez-Saez, G. V.; Pohlabeln, A. M.; Stubbins, A.; Marsay, C. M.; Dittmar, T. Photochemical Alteration of Dissolved Organic Sulfur from Sulfidic Porewater. *Environ. Sci. Technol.* **2017**, *51* (24), 14144–14154. https://doi.org/10.1021/acs.est.7b03713.
(12) Stubbins, A.; Dittmar, T. Illuminating the Deep: Molecular Signatures of Photochemical Alteration of Dissolved Organic Matter from North Atlantic Deep Water. *Mar. Chem.* **2015**, *177* (2), 318–324. https://doi.org/10.1016/j.marchem.2015.06.020.
(13) Antony, R.; Willoughby, A. S.; Grannas, A. M.; Catanzano, V.; Sleighter, R. L.; Thamban, M.; Hatcher, P. G. Photo-Biochemical Transformation of Dissolved Organic Matter on the Surface of the Coastal East Antarctic Ice Sheet. *Biogeochemistry* **2018**, *141* (2), 229–247. https://doi.org/10.1007/s10533-018-0516-0.
(14) Herzsprung, P.; Hertkorn, N.; Friese, K.; Schmitt-Kopplin, P. Photochemical Degradation of Natural Organic Sulfur Compounds (CHOS) from Iron-Rich Mine Pit Lake Pore Waters--an Initial Understanding from Evaluation of Single-Elemental Formulae Using Ultra-High-Resolution Mass Spectrometry. *Rapid Commun. Mass Spectrom. RCM* **2010**, *24* (19), 2909–2924. https://doi.org/10.1002/rcm.4719.
(15) Hoffmann, E. H.; Tilgner, A.; Schrödner, R.; Bräuer, P.; Wolke, R.; Herrmann, H. An Advanced Modeling Study on the Impacts and Atmospheric Implications of Multiphase Dimethyl Sulfide Chemistry. *Proc. Natl. Acad. Sci.* **2016**, *113* (42), 11776–11781. https://doi.org/10.1073/pnas.1606320113.
(16) King, G. M.; Klug, M. J. Sulfhydrolase Activity in Sediments of Wintergreen Lake, Kalamazoo County, Michigan. *Appl. Environ. Microbiol.* **1980**, *39* (5), 950–956.
(17) Laszakovits, J. R.; Berg, S. M.; Anderson, B. G.; O'Brien, J. E.; Wammer, K. H.; Sharpless, C. M. P-Nitroanisole/Pyridine and p-Nitroacetophenone/Pyridine Actinometers Revisited: Quantum Yield in Comparison to Ferrioxalate. *Environ. Sci. Technol. Lett.* **2016**, *4*, 11–14. https://doi.org/10.1021/acs.estlett.6b00422.
(18) Ksionzek, K. B.; Lechtenfeld, O. J.; McCallister, S. L.; Schmitt-Kopplin, P.; Geuer, J. K.; Geibert, W.; Koch, B. P. Dissolved Organic Sulfur in the Ocean: Biogeochemistry of a Petagram Inventory. *Science* **2016**, *354* (6311), 456–459. https://doi.org/10.1126/science.aaf7796.
(19) Cutter, G. A.; Cutter, L. S.; Filippino, K. C. Sources and Cycling of Carbonyl Sulfide in the Sargasso Sea. *Limnol. Oceanogr.* **2004**, *49* (2), 555–565. https://doi.org/10.4319/lo.2004.49.2.0555.
(20) Fimmen, R. L.; Cory, R. M.; Chin, Y.-P.; Trouts, T. D.; McKnight, D. M. Probing the Oxidation-Reduction Properties of Terrestrially and Microbially Derived Dissolved

589 Organic Matter. *Geochim. Cosmochim. Acta* **2007**, *71* (12), 3003–3015.
590 https://doi.org/10.1016/j.gca.2007.04.009.
591 (21) Liu, Z.-Q.; Shah, A. D.; Salhi, E.; Bolotin, J.; von Gunten, U. Formation of Brominated
592 Trihalomethanes during Chlorination or Ozonation of Natural Organic Matter Extracts and
593 Model Compounds in Saline Water. *Water Res.* **2018**, *143*, 492–502.
594 https://doi.org/10.1016/j.watres.2018.06.042.
595 (22) Sleighter, R. L.; Chin, Y.-P.; Arnold, W. A.; Hatcher, P. G.; McCabe, A. J.; McAdams, B.
596 C.; Wallace, G. C. Evidence of Incorporation of Abiotic S and N into Prairie Wetland
597 Dissolved Organic Matter. *Environ. Sci. Technol. Lett.* **2014**, *1* (9), 345–350.
598 https://doi.org/10.1021/ez500229b.
599 (23) Poulin, B. A.; Ryan, J. N.; Nagy, K. L.; Stubbins, A.; Dittmar, T.; Orem, W.; Krabbenhoft,
600 D. P.; Aiken, G. R. Spatial Dependence of Reduced Sulfur in Everglades Dissolved
601 Organic Matter Controlled by Sulfate Enrichment. *Environ. Sci. Technol.* **2017**, *51* (7),
602 3630–3639. https://doi.org/10.1021/acs.est.6b04142.
603 (24) Minor, E. C.; Pothen, J.; Dalzell, B. J.; Abdulla, H.; Mopper, K. Effects of Salinity Changes
604 on the Photodegradation and Ultraviolet—Visible Absorbance of Terrestrial Dissolved
605 Organic Matter. *Limnol. Oceanogr.* **2006**, *51* (5), 2181–2186.
606 https://doi.org/10.4319/lo.2006.51.5.2181.
607 (25) Erickson, P. R.; Moor, K. J.; Werner, J. J.; Latch, D. E.; Arnold, W. A.; McNeill, K. Singlet
608 Oxygen Phosphorescence as a Probe for Triplet-State Dissolved Organic Matter
609 Reactivity. *Environ. Sci. Technol.* **2018**, *52* (16), 9170–9178.
610 https://doi.org/10.1021/acs.est.8b02379.
611 (26) Sharpless, C. M.; Aeschbacher, M.; Page, S. E.; Wenk, J.; Sander, M.; McNeill, K.
612 Photooxidation-Induced Changes in Optical, Electrochemical, and Photochemical
613 Properties of Humic Substances. *Environ. Sci. Technol.* **2014**, *48* (5), 2688–2696.
614 https://doi.org/10.1021/es403925g.
615 (27) Bandstra, J. Z.; Tratnyek, P. G. Central Limit Theorem for Chemical Kinetics in Complex
616 Systems. *J. Math. Chem.* **2005**, *37* (4), 409–422. https://doi.org/10.1007/s10910-004-
617 1107-y.
618 (28) Mostovaya, A.; Hawkes, J. A.; Koehler, B.; Dittmar, T.; Tranvik, L. J. Emergence of the
619 Reactivity Continuum of Organic Matter from Kinetics of a Multitude of Individual
620 Molecular Constituents. *Environ. Sci. Technol.* **2017**, *51* (20), 11571–11579.
621 https://doi.org/10.1021/acs.est.7b02876.
622 (29) Ulshöfer, V. S.; Flock, O. R.; Uher, G.; Andreae, M. O. Photochemical Production and Air-
623 Sea Exchange of Carbonyl Sulfide in the Eastern Mediterranean Sea. *Mar. Chem.* **1996**,
624 *53* (1), 25–39. https://doi.org/10.1016/0304-4203(96)00010-2.
625 (30) Weiss, P. S.; Andrews, S. S.; Johnson, J. E.; Zafiriou, O. C. Photoproduction of Carbonyl
626 Sulfide in South Pacific Ocean Waters as a Function of Irradiation Wavelength. *Geophys.*
627 *Res. Lett.* **1995**, *22* (3), 215–218. https://doi.org/10.1029/94GL03000.
628 (31) Flöck, O. R.; Andreae, M. O. Photochemical and Non-Photochemical Formation and
629 Destruction of Carbonyl Sulfide and Methyl Mercaptan in Ocean Waters. *Mar. Chem.*
630 **1996**, *54* (1), 11–26. https://doi.org/10.1016/0304-4203(96)00027-8.
631 (32) Xie, H.; Moore, R. M. Carbon Disulfide in the North Atlantic and Pacific Oceans. *J.*
632 *Geophys. Res. Oceans* **1999**, *104* (C3), 5393–5402.
633 https://doi.org/10.1029/1998JC900074.

(33) Uher, G.; Andreae, M. Photochemical Production of Carbonyl Sulfide in North Sea Water: A Process Study. *Limnol. Oceanogr.* **2003**, *42* (3), 432–442. https://doi.org/10.4319/lo.1997.42.3.0432.
(34) Pos, W. H.; Riemer, D. D.; Zika, R. G. Carbonyl Sulfide (OCS) and Carbon Monoxide (CO) in Natural Waters: Evidence of a Coupled Production Pathway. *Mar. Chem.* **1998**, *62* (1), 89–101. https://doi.org/10.1016/S0304-4203(98)00025-5.
(35) Andreae, M. O.; Ferek, R. J. Photochemical Production of Carbonyl Sulphide in Marine Surface Waters. *Nature* **1984**, *307* (5947), 148. https://doi.org/10.1038/307148a0.
(36) Zepp, R. G.; Andreae, M. O. Factors Affecting the Photochemical Production of Carbonyl Sulfide in Seawater. *Geophys. Res. Lett.* **1994**, *21* (25), 2813–2816. https://doi.org/10.1029/94GL03083.
(37) Modiri Gharehveran, M.; Shah, A. D. Indirect Photochemical Formation of Carbonyl Sulfide and Carbon Disulfide in Natural Waters: Role of Organic Sulfur Precursors, Water Quality Constituents, and Temperature. *Environ. Sci. Technol.* **2018**, *52* (16), 9108–9117. https://doi.org/10.1021/acs.est.8b01618.
(38) Flöck, O. R.; Andreae, M. O.; Dräger, M. Environmentally Relevant Precursors of Carbonyl Sulfide in Aquatic Systems. *Mar. Chem.* **1997**, *59* (1), 71–85. https://doi.org/10.1016/S0304-4203(97)00012-1.
(39) Powers, L. C.; Miller, W. L. Photochemical Production of CO and CO2 in the Northern Gulf of Mexico: Estimates and Challenges for Quantifying the Impact of Photochemistry on Carbon Cycles. *Mar. Chem.* **2015**, *171*, 21–35. https://doi.org/10.1016/j.marchem.2015.02.004.
(40) Kelly, D. P.; Smith, N. A. Organic Sulfur Compounds in the Environment Biogeochemistry, Microbiology, and Ecological Aspects. In *Advances in Microbial Ecology*; Springer, Boston, MA, 1990; pp 345–385. https://doi.org/10.1007/978-1-4684-7612-5_9.
(41) Hu, H.; Mylon, S. E.; Benoit, G. Distribution of the Thiols Glutathione and 3-Mercaptopropionic Acid in Connecticut Lakes. *Limnol. Oceanogr.* **2006**, *51* (6), 2763–2774. https://doi.org/10.4319/lo.2006.51.6.2763.
(42) Dupont, C. L.; Moffett, James. W.; Bidigare, R. R.; Ahner, B. A. Distributions of Dissolved and Particulate Biogenic Thiols in the Subartic Pacific Ocean. *Deep Sea Res. Part Oceanogr. Res. Pap.* **2006**, *53* (12), 1961–1974. https://doi.org/10.1016/j.dsr.2006.09.003.
(43) Tang, D.; Hung, C.-C.; Warnken, K. W.; Santschi, P. H. The Distribution of Biogenic Thiols in Surface Waters of Galveston Bay. *Limnol. Oceanogr.* **2000**, *45* (6), 1289–1297. https://doi.org/10.4319/lo.2000.45.6.1289.
(44) Cory, R. M.; Kling, G. W. Interactions between Sunlight and Microorganisms Influence Dissolved Organic Matter Degradation along the Aquatic Continuum. *Limnol. Oceanogr. Lett.* **2018**, *3*, 102–116. https://doi.org/10.1002/lol2.10060.
(45) Baker, S. C.; Kelly, D. P.; Murrell, J. C. Microbial Degradation of Methanesulphonic Acid: A Missing Link in the Biogeochemical Sulphur Cycle. *Nature* **1991**, *350* (6319), 627–628. https://doi.org/10.1038/350627a0.
(46) Kelly, D. P.; Murrell, J. C. Microbial Metabolism of Methanesulfonic Acid. *Arch. Microbiol.* **1999**, *172* (6), 341–348. https://doi.org/10.1007/s002030050770.
(47) Henriques, A. C.; Marco, P. D. Methanesulfonate (MSA) Catabolic Genes from Marine and Estuarine Bacteria. *PLOS ONE* **2015**, *10* (5), e0125735. https://doi.org/10.1371/journal.pone.0125735.

(48) McNeill, V. F. Aqueous Organic Chemistry in the Atmosphere: Sources and Chemical Processing of Organic Aerosols. *Environ. Sci. Technol.* **2015**, *49* (3), 1237–1244. https://doi.org/10.1021/es5043707.
(49) Quinn, P. K.; Collins, D. B.; Grassian, V. H.; Prather, K. A.; Bates, T. S. Chemistry and Related Properties of Freshly Emitted Sea Spray Aerosol. *Chem. Rev.* **2015**, *115* (10), 4383–4399. https://doi.org/10.1021/cr500713g.
(50) Quinn, P. K.; Bates, T. S. The Case against Climate Regulation via Oceanic Phytoplankton Sulphur Emissions. *Nature* **2011**, *480* (7375), 51–56. https://doi.org/10.1038/nature10580.
(51) Quinn, P. K.; Coffman, D. J.; Johnson, J. E.; Upchurch, L. M.; Bates, T. S. Small Fraction of Marine Cloud Condensation Nuclei Made up of Sea Spray Aerosol. *Nat. Geosci.* **2017**, *10* (9), 674–679. https://doi.org/10.1038/ngeo3003.
(52) Cheng, Y.; Zheng, G.; Wei, C.; Mu, Q.; Zheng, B.; Wang, Z.; Gao, M.; Zhang, Q.; He, K.; Carmichael, G.; Pöschl, U.; Su, H. Reactive Nitrogen Chemistry in Aerosol Water as a Source of Sulfate during Haze Events in China. *Sci. Adv.* **2016**, *2* (12), e1601530. https://doi.org/10.1126/sciadv.1601530.
(53) Gen, M.; Zhang, R.; Huang, D. D.; Li, Y.; Chan, C. K. Heterogeneous Oxidation of SO2 in Sulfate Production during Nitrate Photolysis at 300 Nm: Effect of PH, Relative Humidity, Irradiation Intensity, and the Presence of Organic Compounds. *Environ. Sci. Technol.* **2019**, *53* (15), 8757–8766. https://doi.org/10.1021/acs.est.9b01623.
(54) Zheng, B.; Zhang, Q.; Zhang, Y.; He, K. B.; Wang, K.; Zheng, G. J.; Duan, F. K.; Ma, Y. L.; Kimoto, T. Heterogeneous Chemistry: A Mechanism Missing in Current Models to Explain Secondary Inorganic Aerosol Formation during the January 2013 Haze Episode in North China. *Atmospheric Chem. Phys.* **2015**, *15* (4), 2031–2049. https://doi.org/10.5194/acp-15-2031-2015.

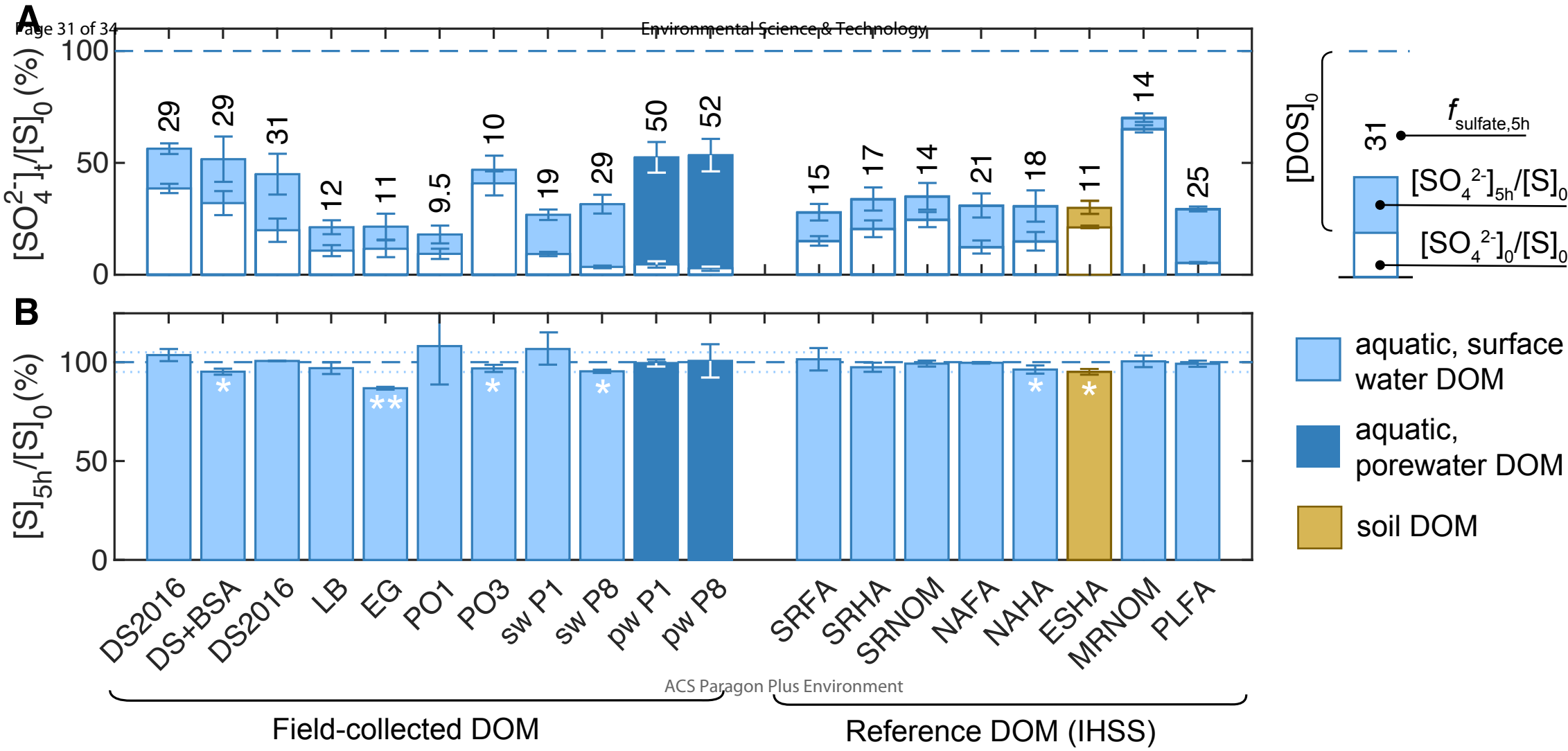

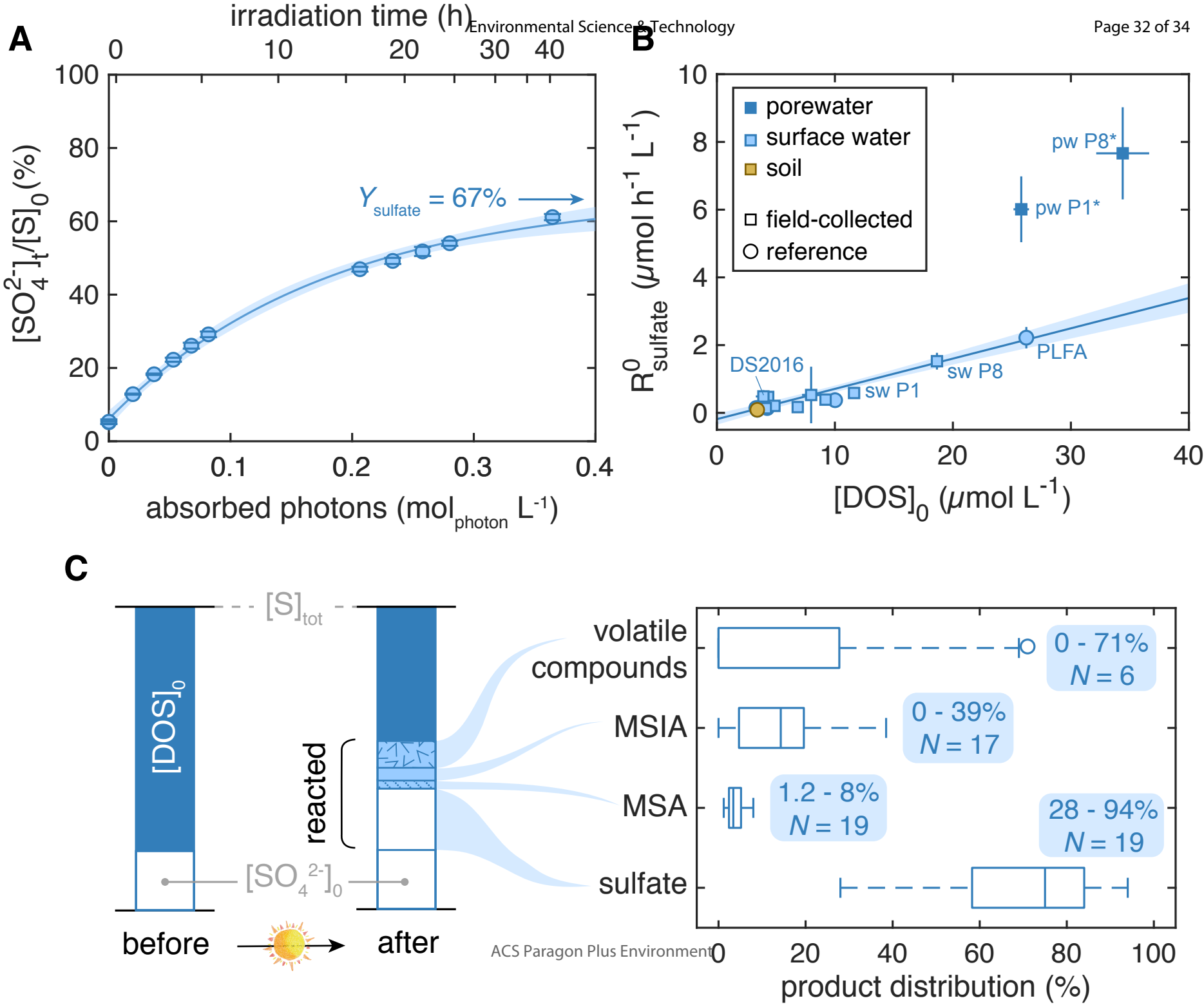
A
irradiation time (h)
0
10
20
30
40
100
80
60
40
20
0
$[SO_4^{2-}]_t/[S]_0$ (%)
$Y_{sulfate}$ = 67%
0
0.1
0.2
0.3
0.4
absorbed photons (mol_{photon} L^{-1})
B
10
8
6
4
2
0
$R^0_{sulfate}$ (μmol h^{-1} L^{-1})
porewater
surface water
soil
field-collected
reference
pw P8*
pw P1*
PLFA
sw P8
sw P1
DS2016
0
10
20
30
40
$[DOS]_0$ (μmol L^{-1})
C
$[S]_{tot}$
$[DOS]_0$
reacted
$[SO_4^{2-}]_0$
before
after
volatile compounds
MSIA
MSA
sulfate
0 - 71%
N = 6
0 - 39%
N = 17
1.2 - 8%
N = 19
28 - 94%
N = 19
0
20
40
60
80
100
product distribution (%)

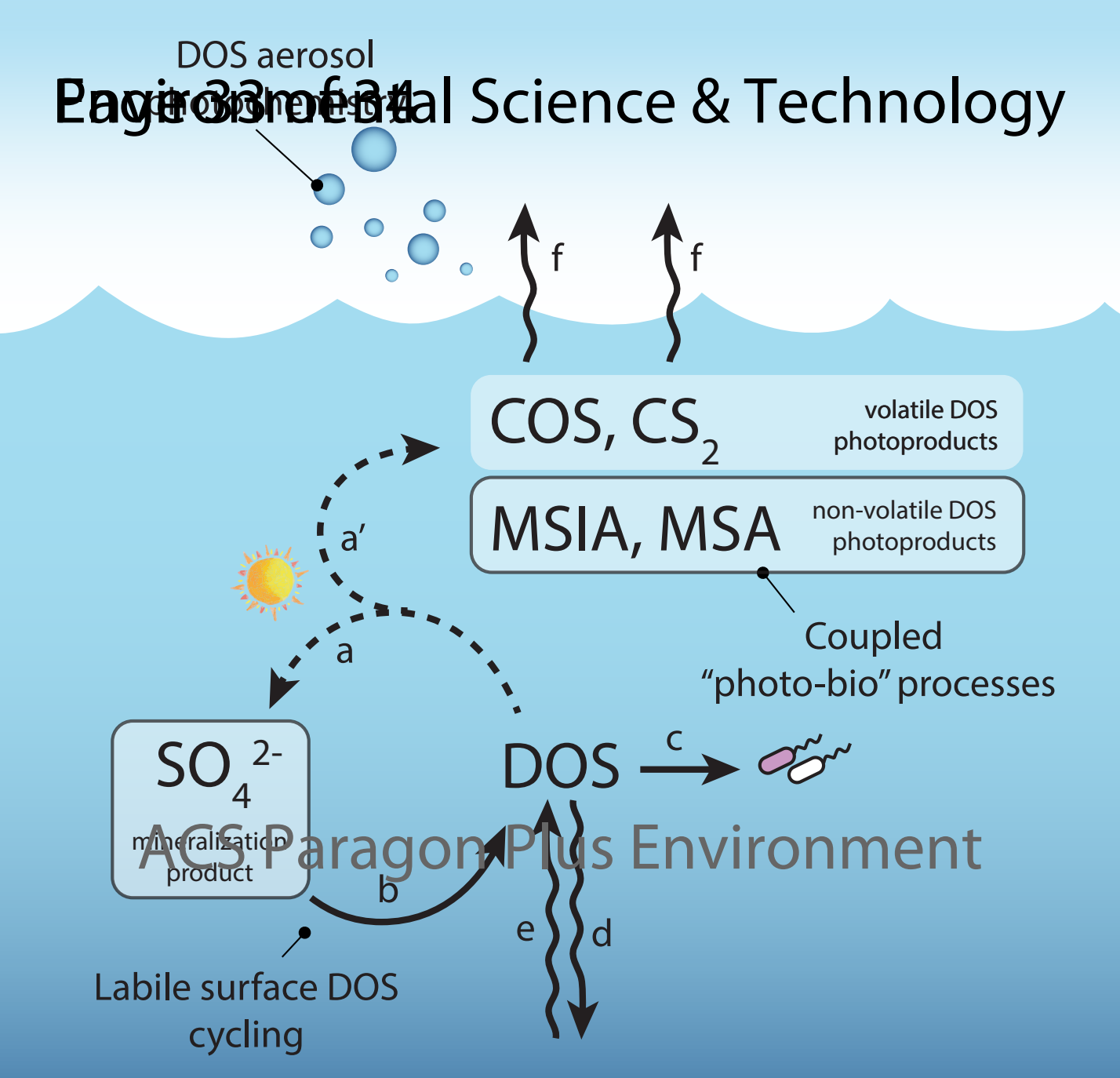

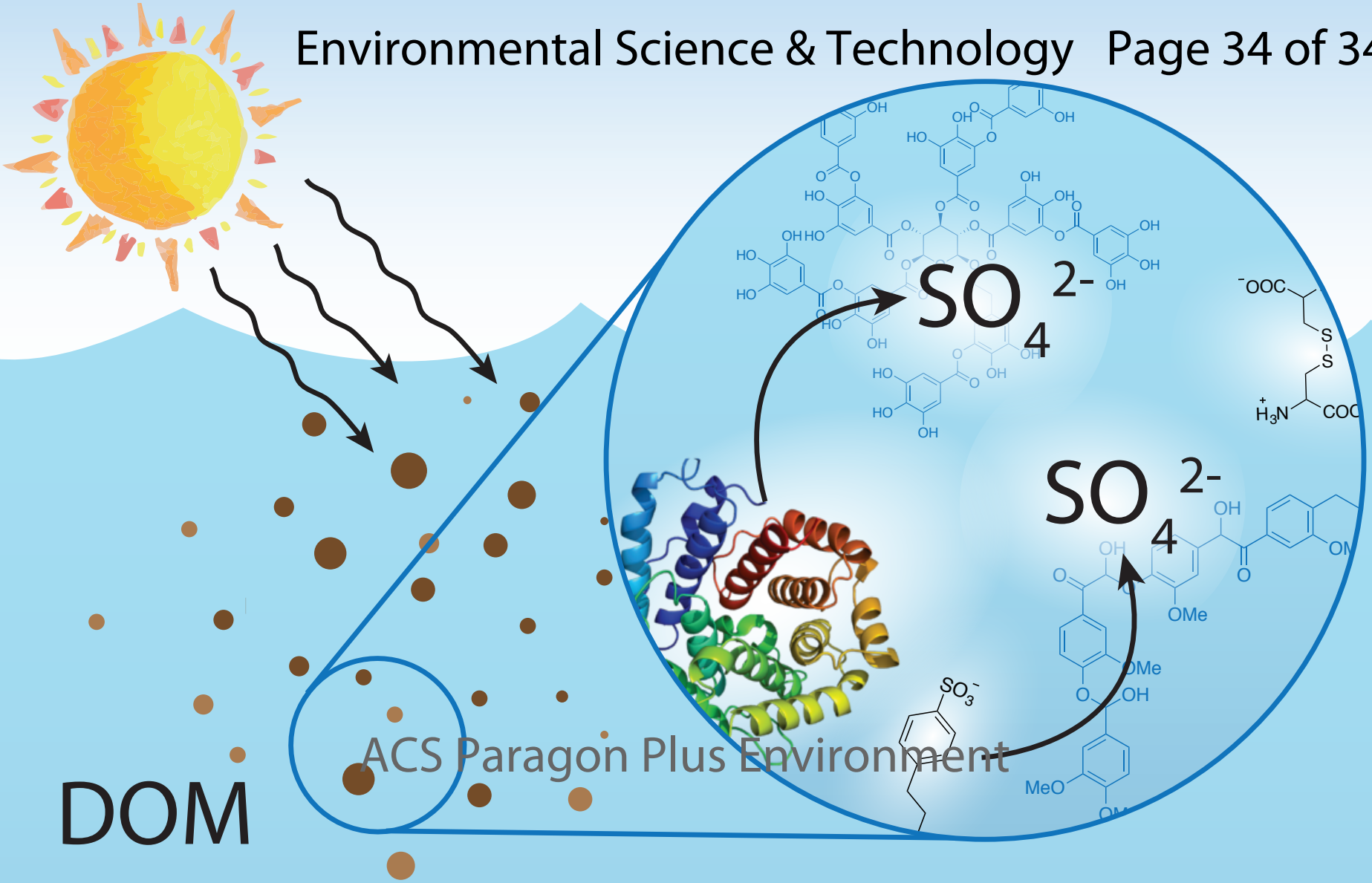
SO4 2-
SO4 2-
DOM
ACS Paragon Plus Environment